86827

12 June 1995

ANL/CHM/PP--86827

Solution Spectroelectrochemical Cell for In Situ X-ray Absorption Fine Structure

Mark R. Antonio* and L. Soderholm

Chemistry Division, Argonne National Laboratory, Argonne, Illinois 60439-4831 U.S.A.

Inho Song

Department of Materials Science and Engineering, The Case School of Engineering, Case Western Reserve University, Cleveland, Ohio 44106-7204 U.S.A.

ABSTRACT

A purpose-built spectroelectrochemical cell for in situ fluorescence XAFS (X-ray Absorption Fine Structure) measurements of bulk solution species during constant-potential electrolysis is described. The cell performance was demonstrated by the collection of europium L_3-edge XANES (X-ray Absorption Near Edge Structure) throughout the course of electrolysis of an aqueous solution of $EuCl_3 \cdot 6H_2O$ in 1 M H_2SO_4. The europium L_3-edge resonances reported here for the Eu^{III} and Eu^{II} ions demonstrate that their $2p_{3/2} \rightarrow 5d$ electronic transition probabilities are *not* the same.

MASTER

INTRODUCTION

XAFS (X-ray absorption fine structure) spectroscopy has found widespread application for in situ studies of systems of electrochemical interest. The combination of XAFS and electrochemical methods provides direct insights about electroactive species that are otherwise unavailable through use of the individual techniques alone. For example, XAFS spectroelectrochemistry has been used to probe the coordination and chemistry of adsorbed species, electrode/electrolyte interfaces, insoluble oxide films produced by passivation and corrosion, battery electrode materials, electrocatalysts, electrochemically-generated complexes in solution, etc.[1-6] The investigation of these fundamental phenomena and practical devices has been facilitated by the development of novel electrochemical cells that have proven to be suitable for a variety of XAFS measurements under electrochemically-relevant conditions.[4,7-22] Based upon the science of interest, it is important to utilize the appropriate spectroelectrochemical cell design to accomplish the task at hand. For our particular studies of the redox behavior of lanthanide cations and heteropolyoxometalate anions in aqueous electrolytes, we make use of a purpose-built cell for in situ XAFS data acquisition during bulk electrolysis at controlled potentials. This new, bulk electrolysis spectroelectrochemical cell design is described. The cell performance is illustrated by following the course of the constant potential reduction of Eu^{III} to Eu^{II} in an aqueous mineral acid solution through europium L_3-edge XANES (X-ray absorption near edge structure) measurements. The europium(III,II) system has a simple and well-understood Pourbaix diagram.[23] Furthermore, the standard formal reduction potential of -0.55 V vs Ag/AgCl is attainable in aqueous, noncomplexing supporting electrolytes.[24-27] As such, the Eu(III,II) redox couple serves as an excellent model system to illustrate the application of this original solution spectroelectrochemical cell design.

EXPERIMENTAL SECTION

Electrochemical Cell Design. An assembly drawing of the solution spectroelectrochemical cell for bulk electrolysis and in situ XAFS experiments is shown in Figure 1. There are three main components of this design: [1] the solution cell (H) with its attachments (A-E, I-K, M); [2] the cell positioner (N) with the cell attachments (A-D), and; [3] the cell box (F) with its components (G, L, O). A complete description of the items (A-O) illustrated in Figure 1, including the principal dimensions, is provided in Table I. The working (A) and auxiliary (D) electrodes are held in the cell body (H) and in the cell positioner (N) by four nylon male connectors (Swagelok, bored-through fitting, NY-6MO-1-2BT, 6 mm tube to 1/8 in. pipe thread). The separation between the centers of the two graphite rods (A and D) is 1-1/2 in. The holes in the aluminum positioner (N) provide ample clearance to prevent contact with the electrodes. The two male connectors on the cell positioner (N) permit the vertical alignment of the X-ray beam on the cell window (J). The positioner (N) can be rotated through 360° to allow adjustment of the angle between the cell and the incident X-ray beam. Once aligned, the positioner (N) can be locked down with two chocks (not shown) on the top of the box (F). The reference electrode (E) port in the cell (H) was drilled for a slip fit. The electrode (BAS, Inc., MF-2063) was held at the proper depth with an O-ring seal, not shown in Figure 1. For this study, a chloride-containing reference electrode (E) was placed directly in the working electrode compartment. This is an acceptable configuration for electrolyte solutions of chloride salts of transition-metal ion and lanthanide complexes. For other applications where contamination of the electrolyte by Cl^- is of concern, the reference electrode can be placed outside the cell and connected to a luggin capillary inside the cell (H) through a cracked stopcock bridge. Alternatively, a non-chloride based reference electrode (e.g., Ag/Ag_xS_y, $Cu/CuSO_4$, Hg/HgO, reversible hydrogen electrode, etc.) can be used in place of the presently used Ag/AgCl reference electrode. The connecting lead wire

(not shown) was brought down to the 0.060 in. reference electrode pin through a feed port (not shown) in the cell positioner (N). The Teflon™ feed tube (C) for gas purging is held in the cell positioner (N) and the cell (H) by two nylon male connectors (Swagelok, bored-through fitting, NY-100-1-1BT, 1/16 in. tube to 1/16 in. pipe thread). The drilled-through holes in the cell positioner (N) and the cell (H) were of adequate clearance to facilitate easy insertion of the Teflon™ feed tube (C). Active and vigorous purging through tube (C) was used to effect stirring. Blanketing the solution with gas was done with the tube (C) withdrawn above the electrolyte level. The gas vent/electrolyte feed tube (B) was brought through the cell positioner (N) with a slip fit hole and through the cell (H) with a press fit hole. The tube (B) is used for filling the cell and for venting the purge gas and other gases that may be produced at the electrodes during the electrolysis. The compartment (M) for the auxiliary electrode (D) was made to stand off of the bottom of the cell (H) by ca. 2 mm. Five equally-spaced arches were formed at the end of the tubular auxiliary electrode compartment (M). These open slots provide low resistance current passage. The glass frit (pore d. 10-20 μm) in the bottom end of the auxiliary electrode compartment (M) prevents the direct mixing of the electrolytes between the working (A) and auxiliary electrode (D) compartments. The auxiliary compartment tube (M) fits snugly within the 1 in. vertical opening in the cell (H). However, because there is no seal between the cell (H) and the top of the auxiliary electrode compartment (M), the electrolyte can spill over into the auxiliary compartment if the cell is filled to capacity. In order to prevent intermixing of anolyte and catholyte, the best electrolysis volumes were found to range from 5 to 7 cm^3—this includes the volume of electrolyte in the auxiliary electrode compartment. O-ring seals (I) were pressed into the channels on both sides of H (only one side is shown in Figure 1) to provide a leak-tight seal of the window film (J) with the cell (H). The use of Kalrez O-ring seals, although expensive, provided the best leak-tight seals. Other materials, especially

rubber, were more prone to swelling and cracking by the use of aggressive supporting electrolytes. The window frame (K) had a raised (1/32 in.) rim on the inside surface that mated with the cell (H) to provide a snug, snap fit of the window film (J) into the cell (H). The window film was secured by the window frame (K) with eight screws (#4-40 x 1 in., allen head) and nuts, not shown in Figure 1. We found that 5 μm polycarbonate film provides satisfactory chemical resistance and, at the same time, has excellent transmission characteristics for low energy (i.e., long wavelength) X-radiation.[28] In fact, we routinely use this film for phosphorus K-edge (2,130 eV) XAFS.[29] Although it provides good service for our applications, it is not as strong nor as resistant to chemical attack as other commercially available films of Kapton™, Mylar™, etc. The position and height of the X-ray entrance/exit windows (L) in the cell box (F) were machined to match the position and height of the windows in a commercially available housing (The EXAFS Co., Pioche, NV), which was designed to contain a reactor/furnace for in situ XAFS studies of heterogeneous catalysts under industrially-relevant conditions. The complete spectroelectrochemical cell assembly (the cell (H) and the cell positioner (N) with all connecting parts) can be directly inserted and is precisely accommodated within this catalysis reactor housing. As such, the reactor housing can be used to contain the presently reported cell for in situ XAFS spectroelectrochemistry experiments. The mounting bracket (G) was designed to provide an exact fit with a commercially available fluorescent X-ray ion chamber detector (The EXAFS Co., not shown). This bracket can be substituted with a soller slit assembly (The EXAFS Co.). Directly behind the mounting bracket (G), on the inside of the box, are two vertical guides (not shown in Figure 1) that are used to accommodate large area fluorescence filters (10 cm x 10 cm) available from EXAFS Materials (Danville, CA). The cell box (F) has two purge ports (O) so that it can be flooded with helium to minimize absorption of incident and fluorescent X-radiation.

Apparatus and Reagents. A potentiostat (BAS, CV-27 voltammograph) was used for the constant-potential electrolysis of a 14.2 mM $EuCl_3 \cdot 6H_2O$ (Aldrich) solution in a 1 M H_2SO_4 (Fisher Scientific, Optima) aqueous supporting electrolyte prepared with deionized water (18 MΩ-cm). This solution (7 cm^3) was injected into the spectroelectrochemical cell where it was purged with helium prior to and throughout the course (ca. 7 h) of electrolysis and in situ XANES. From the open circuit potential (0.4 V vs Ag/AgCl), the electrode polarization was stepped to -0.7 V vs Ag/AgCl for the bulk electrolysis experiment. All quoted potentials are given with respect to a silver/silver chloride (SSC) reference electrode in a 3 M NaCl aqueous solution. The illumination of the spectroelectrochemical cell with the X-ray beam had no effect on either the control or measurement of the current and potential during the electrolysis process.

XANES Data Collection. Europium L_3-edge XANES was collected at ambient temperature on beamline X-23A2 at the National Synchrotron Light Source. X-23A2 is equipped with a Si<311> double crystal monochromator, which provides an energy resolution of $\delta E/E = 2.90 \times 10^{-5}$,[30] and effective harmonic rejection of the second order Bragg reflection. The feedback system was adjusted provide ca. 90% the maximum incident X-ray intensity I_0 (to suppress third order harmonic contamination) throughout the Eu L_3-edge scan. The europium fluorescence signal was detected by use of a flow-type ion chamber detector (The EXAFS Co.) purged with argon and without slits or filters. Nitrogen was used to monitor I_0, and helium was used to purge the spectroelectrochemical cell box. The horizontal beam width on the cell window was 15 mm in the conventional 45°-incident/45°-exit fluorescence XAFS configuration. With a 1 mm pre-monochromator vertical slit, a total energy bandwidth of 1.1 eV at 7,000 eV is realized. This was approximated by the square root of the quadratic sum of the monochromator rocking curve width ($2\delta E^2 = 0.082$ eV) and the X-ray beam divergence ($\Delta E^2 = 1.2$ eV).[31] Because the instrumental resolution (1.1 eV)

is some 3-1/2 times smaller than the natural linewidth (3.91 eV) of the Eu L_3 core hole,[32] the Eu L_3-edge XANES shown here is only slightly broadened (ca. 4%) by the optical elements of the beamline. The in situ XANES was recorded, first, at the open circuit potential and, then, throughout the course of the electrolysis with the electrode polarized at -0.7 V vs SSC. The L_3-edge region was scanned with a step size of 0.3 eV/pt at 4 s/pt—a single scan from 6,850 to 7,620 eV took 32 min. The scan-to-scan energy calibration was maintained to ±0.2 eV. The calibration was set with reference to the inflection point energy (6980.3 eV) in the first differential, transmission XANES of a standard EuF_3 absorber (EXAFS Materials). The normalization of the XANES to a unit edge jump was performed according to conventional methods.[31] The pre-edge (6,850-6,955 eV) background was approximated by a two-term linear function, and the post-edge (7,000-7600 eV) background was approximated by a three-term quadratic function. As described elsewhere,[33-37] the normalized XANES was fit with the sum of Lorentzian and arctangent functions convolved with a 1.2 eV Gaussian broadening function to account for the effect of the X-ray beam divergence.

RESULTS

The spectra of Figure 2 show the evolution of the Eu L_3-edge XANES throughout the 7 hr electrolysis of the aqueous solution of $EuCl_3 \cdot 6H_2O$ in the spectroelectrochemical of Figure 1. The normalized Eu XANES for this colorless, deaerated solution at open circuit potential reveals a single, intense edge resonance at ca. 6,982 eV. It is characteristic of Eu^{III}, which has the descriptive ground state electronic configuration of $[Xe]4f^6 5d^0 6s^0$. The resonance is the result of an electronic transition from the Eu $2p_{3/2}$ manifold to the empty 5d manifold. With the commencement of electrolysis at -0.7 V vs SSC, the first of a series of XAFS scans was begun. This first scan (t = 0, Figure 2) reveals the growth of a small shoulder near the

base of the Eu^{III} resonance. With increasing electrolysis times (t = 1.2 and 2.8 h), this shoulder develops into a new and well-resolved edge resonance at ca. 6,974 eV. At the same time, the intensity of the Eu^{III} resonance decreases. The new edge resonance, which is some 8 eV below the Eu^{III} resonance, is characteristic of Eu^{II},[38-43] which has the $[Xe]4f^75d^06s^0$ electronic configuration. After 7 h of electrolysis, the Eu^{II} resonance dominates the spectrum, although there is some indication for the presence of residual Eu^{III}. From the data of Figure 2, it is clear that Eu L_3-edge XANES provides direct information about the valence of Eu. The fits to the normalized XANES for the pure Eu^{III} and Eu^{II} solutions, and the individual components of the fits are displayed in Figure 3. The curve fitting results for the Eu^{II} and Eu^{III} oxidation states as well as for one of the $Eu^{II,III}$ mixtures (t = 2.8 h) are available in Table II.

DISCUSSION

The first solution cell employed for XAFS spectroelectrochemistry had a thin-layer working electrode design that facilitated rapid, exhaustive electrolysis of small analyte volumes, ca. 500 μL.[8,9] A flow-cell, bulk electrolysis system for in situ XAFS with a large analyte capacity (ca. 10 cm^3) was recently shown to be effective for controlling the oxidation state of transition metal ions in complexes such as $[Co(2,2'\text{-bipyridine})_3]^{n+}$, for n=2 and 3.[10] The characteristic features of all solution spectroelectrochemical cells of published design[8-10] are their large electrode-area-to-solution-volume ratios (A/V) and, hence, their rapid electrolytic conversion times, less than approximately 10 min. The design of Figure 1 is the result of our effort to produce a cell of intermediate analyte volume (ca. 5 cm^3) that facilitates time-dependent observations of lanthanide redox processes that can be made to proceed slowly (i.e., several h) over the course of a conventional XAFS scan of ca. 30-50 min. As demonstrated by the in situ Eu XANES of Figure 2, which reveals the evolution of

the reduction of Eu^{III} during electrolysis for ca. 7 h, the reported cell design permits experiments of fairly long duration precisely because of the intended small A/V condition. Because the cell was designed for electrolysis over extended time periods, it was essential to separate the working and auxiliary electrodes in order to provide exact control of the electrochemical conditions.[44] This was accomplished by use of a fritted auxiliary electrode compartment, which provides isolation of anolyte and catholyte and, thereby, eliminates their direct intermixing and the possibility of undesirable reactions between them. Most important, with careful alignment, the incident X-ray beam can be directed onto the electrolyte in the working electrode compartment. The resulting X-ray fluorescence signal from the analyte of interest will be free of spectral contamination from species generated within the auxiliary electrode compartment. This is a key feature of the design of Figure 1.

For the $Eu^{III} + e^- \rightarrow Eu^{II}$ reaction as followed here, the cathodic reduction product (e.g., Eu^{II}) was illuminated within the working electrode compartment. The diffusion of Eu^{II} to the auxiliary electrode, where oxidation to Eu^{III} would occur, was restricted by the frit separator. Anodic oxidation products (e.g., O_2, Eu^{III}) within the auxiliary electrode compartment were not illuminated. The separator restricts their diffusion through the X-ray illuminated electrolyte to the working electrode where they would alter the electrolyte composition and prevent the electrolysis from reaching completion. By comparison, with a thin-layer, parallel plate electrode geometry, the X-ray beam would illuminate both the working and auxiliary electrodes. The resulting spectral response would be an average of both the anolyte and catholyte signals. A parallel plate cell design might be more problematic for transmission XAFS measurements than for fluorescence XAFS measurements. The fluorescence signal could contain contributions from both the anolyte and catholyte—the exact extent of the combination of different responses depends upon the fluorescence energy and the position of the auxiliary electrode.

The error in measurement and control of electrode potential for the cell design of Figure 1 was minimized through the placement of the working and reference electrodes in close proximity (1/4 in. separation), and by use of a supporting electrolyte with high conductivity. Finally, the spectroelectrochemical system was purposely designed for direct operation with commercially-available detectors, slits, filters, and catalyst cell housings that are now in widespread use at many synchrotron radiation facilities throughout the world.

Although the 14.2 mM analyte (Eu) concentration examined here is rather high for analytical electrochemistry, the data of Figure 2 demonstrate that it is a practical concentration for the acquisition of good quality XANES in a single scan. In view of the stability of Eu^{II} as well as the attainable standard reduction potential for Eu^{III} (E^0 = -0.55 V vs SSC in acid solution[24,27]), this solution system provided an ideal test of the new spectroelectrochemical cell. We have used this cell for other in situ XANES studies as well. For example, in situ XANES was obtained for several lanthanide-exchanged heteropolyoxotungstate anions of composition $[LnP_5W_{30}O_{110}]^{n-}$.[36,45] For the Eu^{III}-exchanged anion (5 mM in an aqueous electrolyte of 1 M H_2SO_4), we demonstrated that europium is electroactive and reducible to Eu^{II} after electrolysis at -0.55 V vs SSC for 1 h.[45] Although the cell was designed for fluorescence measurements, the back cell window is X-ray transparent to permit transmission XAFS measurements. The disadvantage here is that the fixed cell body thickness, 1/2 in., restricts its use for transmission XAFS to high energy experiments, such as for the K-edge of Cs (35,985 eV) and beyond. In fact, from proof-of-concept measurements conducted at SSRL with a Si<400> monochromator on beamline IV-2, we have demonstrated that this cell provides the ideal absorber thickness for Cs K-edge transmission XAFS of 0.1 M aqueous solutions of $CsNO_3$ and CsCl.[46]

The Eu XANES data reported here were all obtained from the same dilute analyte in aqueous solution. Because of the low absorber concentration, the peak

intensities are not vitiated by thickness effects, which can oftentimes cause serious distortions of intense $L_{2,3}$-edge resonances obtained from concentrated, solid-state samples.[31,47] Therefore, the curve fitting of the Eu $L_{2,3}$-edge XANES of Figure 2 yields quantitative information about the resonance energies, widths, and intensities—all of which provide insights about the electronic properties of the absorbing Eu ion. The 8 eV difference in the europium edge-resonance energies between the solution species at open circuit potential before electrolysis and at -0.55 V vs SSC after electrolysis is sufficient to assign the oxidation states of Eu^{III} at rest potential and Eu^{II} in the reduced solution. This interpretation of the XANES results is consistent with a variety of other published studies of Eu compounds.[38-43,48] The Eu^{III}-Eu^{II} edge-resonance energy difference is also in line with that observed for the Ln^{III} and Ln^{II} L_3 XANES of other lanthanide ions, including Nd, Sm, and Yb.[49-52] Similarly, a 7–9 eV difference has been previously observed between Eu^{II} and Eu^{III} resonances in Eu $3d_{5/2}$ XPS (X-ray photoelectron spectroscopy) data.[53-55]

The integrated intensity of an L_3-edge resonance is proportional to its oscillator strength, which includes a radial dipole-moment integral as well as the density of 5d states with the appropriate symmetry.[34,56] It has been previously reported that the width of an L_3-edge resonance varies with the atomic volume of the lanthanide[48,57] presumably through changes in the radial component of the oscillator strength. Rescaling the relative Eu^{III} and Eu^{II} energies, by a squared-ratio of their ionic radii, to account for this volume effect, produces a trivalent linewidth similar to that observed for the divalent ion. Therefore, the increased linewidth of the Eu^{III} resonance over that of the Eu^{II} resonance observed here (Table II) is attributed primarily to the difference in the atomic volume of these two ions.

As seen from Figure 3, and shown in Table II, the intensity of the electronic transition for Eu^{III} is also considerably larger than that for Eu^{II}. Whereas the decreased radial integral expected for Eu^{II} versus Eu^{III} is expected to decrease the

observed intensity, differences in the density of 5d final states will also play a role. Eu^{III} has a $4f^65d^0$ configuration. It has been clearly demonstrated that there is very little 4f-5d hybridization or configuration mixing in this ion. The 4f valence states are separated by about 8.5–9 eV from the unoccupied 5d states.[58] However, for the Eu^{II} ion, the outer electrons are subjected to a much smaller effective nuclear charge, which results in much smaller separations between configurations. The Eu^{II} ($4f^75d^0$) 4f-5d separation has been found to be about 2.5 eV for the free ion.[58,59] The effect of the crystal field is also larger for the divalent europium f-ion, and is expected to be of the same order as the free-ion splitting. These combined effects result in significant 4f-5d hybridization for Eu^{II}, giving some f character to the 5d states. This reduces the density of final-state holes with the symmetry appropriate for the L_3-edge transition, thereby contributing to the decrease in observed intensity of the Eu^{II} resonance compared to that of the Eu^{III} resonance.

Whereas the larger ionic radius and the increased hybridization of the Eu^{II} ion are both expected to contribute to the decease in the observed intensity of the Eu^{II} L_3-edge-resonance over that of the Eu^{III} resonance, their relative effects cannot be ascertained without further work. The observation of a decreased amplitude for the Eu^{II} resonance has been previously reported by Ravot et al.[40], who note that the amplitude of the Eu L_3-edge-resonance in $Eu^{II}O$ is about 1.5 times smaller than that for $Eu_2^{III}O_3$. This ratio is similar to the one reported here in Table II. Further support for a difference between Eu^{II} and Eu^{III} L_3-edge-resonance intensities is indicated from a study in which relative Eu^{II}/Eu^{III} concentrations were estimated from both L_3-edge XANES and ^{151}Eu Mössbauer spectra. The relative Eu^{II}/Eu^{III} concentrations obtained from the XANES data were found to be different from those obtained from the Mössbauer data.[60]

Our results reported here provide unambiguous evidence of the decreased $L_{2,3}$-edge absorption intensities observed for Eu^{II} over that of Eu^{III} because the

XANES data were obtained *on the same sample*. This is a particularly important result because XANES studies are used to determine the fractional valence in Eu homogeneous mixed-valent systems. These studies often rely on the assumption that the transition probabilities of the Eu^{II} and Eu^{III} are the same [see for example, Rohler[48]], but the work reported here shows that this assumption is not valid.

ACKNOWLEDGMENT

We thank Donald Sutter, Greg Ktistou, and Joe Gregar (ANL) for their expert fabrication of this spectroelectrochemical cell. A part of this research was conducted at the National Synchrotron Light Source, which is supported by the U.S. Department of Energy, Division of Material Sciences and Division of Chemical Sciences. This work was supported by the U.S. D.O.E., Basic Energy Sciences—Chemical Sciences, under contract W-31-109-ENG-38.

DISCLAIMER

Table I. Descriptions, part numbers (where available), quantities (Qty), and principal dimensions of items A-O used for the fabrication of the XAFS spectroelectrochemical cell shown in Figure 1.

Items	Part No.	Description	Qty
A, D	14739	Carbon rod, 6.15 mm d. x 300 mm, Purity Grade "F"; Material Grade AGKSP (Alfa)	2
B, C	Z11731-5	Syringe Needle, 20-Gauge Teflon™, 12 in. long, with Kel-F Luer Hub (Aldrich)	2
E	MF-2063	Ag/AgCl reference electrode (5.5 cm x 6 mm o.d.) with porous Vycor™ tip and 3 M NaCl, RE-5 (BAS)	1
F		Cell Box (8-9/16 x 5-1/4 x 3-7/16 in.), aluminum, with removable Plexiglas cover	1
G		Detector Bracket (4-7/16 x 4-7/16 x 1 in.), aluminum, to support fluorescent ion chamber detector	1
H		Cell Body (2-3/8 x 2-3/8 x 1/2 in.) , Kel-F	1
I	AS-568A	O-Ring, Kalrez, K#031, Compound 4079, 1-3/4 x 1-7/8 x 1/16 in. (DuPont)	2
J	3522	Polycarbonate Window Film, 0.20 mil thick (SPEX)	2
K		Cell Window Frame (2-3/8 x 1-25/32 x 5/32 in.), Plexiglas	2
L		Slot (2-1/2 x 5/16 in.), covered with polycarbonate window film (Item J)	2
M	7205-SP-10MMD	Fritted cylindrical sealing tube, porosity D, 10 mm o.d. (Ace Glass)	1
N		Cell Positioner (2-13/16 i.d. x 3-1/16 in. o.d.), Aluminum	1
O	268-P-04x02	Male Connector, Poly-Flow (Imperial Eastman), 1/4 in. tube to 1/8 in. pipe thread	2

Table II. Europium L_3-edge Peak Intensities of the Normalized XANES Displayed in Figure 1 and the Results (Positions, Heights, FWHMs, Areas, Offsets) from the Curve-Fitting Analysis of the Normalized XANES.[a]

	Eu^{III} | Eu^{II} Edge Resonances					Edge Steps			
Time[b]	Intensity	Position	Height	FWHM	Area	Position	Height	FWHM	Offset
BE[c]	4.15	6981.9	4.33	4.70	32.0	6986.4	0.78	7.30	-0.09
2.8	2.05 | 2.12	6981.8 | 6973.7	1.81 | 2.03	5.88 | 4.28	16.7 | 13.7	6987.0	1.10	6.74	-0.07
7.0	3.04	6973.7	3.08	4.33	21.0	6977.0	1.03	5.30	-0.06

[a] The Eu^{III} and Eu^{II} edge resonances, due to $2p_{3/2} \rightarrow 5d$ bound-state electronic transitions, were modeled with Lorentzian functions and the absorption edge steps were modeled with arctangent functions by use of the algorithm of Lytle et al. (EDGFIT).[33,34] A second Lorentzian function was added to approximate the post-edge (EXAFS) peaks in order to provide better fits to the overall spectra obtained before electrolysis (BE) and after 7 h of electrolysis, see Figure 3. [b]Times are in hours from the start of the electrolysis with the electrode polarized at -0.7 V vs SSC. [c]Solution before electrolysis at open circuit potential.

FIGURE CAPTIONS

Figure 1. Assembly drawing of the spectroelectrochemical system for *in situ* XAFS measurements. A: Working electrode; B: Electrolyte feed tube and gas vent port; C: Purge gas feed tube; D: Working electrode; E: Reference electrode; F: Cell box; G: Bracket for mounting a fluorescence detector (not shown); H: Spectroelectrochemical cell; I: O-ring seal; J: Cell window; K: Window frame; L: X-ray windows; M: Auxiliary electrode compartment; N: Cell positioner; O: Cell box purge ports. In this view, the spectroelectrochemical cell is shown at a 45° angle, as it would be used for fluorescence XAFS measurements with the incident X-ray beam entering the cell box from the right. For clarity, the eight screws (#4-40 x 1 in., allen head, and nuts) for mounting the cell window and the back side window disassembly are not shown.

Figure 2. In situ europium L_3-edge XANES spectroelectrochemistry of $EuCl_3 \cdot 6H_2O$ (14.2 mM) in an aqueous supporting electrolyte of 1M H_2SO_4 at open circuit potential (0.4 V vs SSC) and after bulk electrolysis with the electrode polarized at -0.7 V vs SSC for 0, 1.2, 2.8, and 7.0 h. The bulk electrolysis and the first scan were started simultaneously. The small Eu^{II} contribution noted in the spectrum labeled t = 0 was produced in the short time taken to go from the start of the scan at 6,850 eV to ca. 6,970 eV. The faint vertical lines at 6973.6 and 6981.6 eV indicate the position of the Eu^{II} and Eu^{III} edge resonances, respectively.

Figure 3. The normalized XANES (dots) for the 14.2 mM aqueous solution of $EuCl_3 \cdot 6H_2O$ in 1M H_2SO_4 obtained at open circuit potential (Eu^{III}, top) and after constant potential bulk electrolysis for 7 h with the electrode polarized at -0.7 V vs SSC (Eu^{II}, bottom). The fits to the data are shown as solid lines and the individual Lorentzian and arctangent components of the fits are shown as dashed lines.

LITERATURE CITED

(1) *Electrochemical Interfaces. Modern Techniques for In-Situ Interface Characterization*; Abruna, H. D., Ed.; VCH Publishers: New York, 1991.

(2) *Structure of Surfaces and Interfaces as Studied Using Synchrotron Radiation;* Faraday Discussions of The Chemical Society; The Royal Society Of Chemistry: London, 1990; Vol. 89.

(3) *Proceedings of the Symposium on X-ray Methods in Corrosion and Interfacial Electrochemistry*; Davenport, A.; Gordon, J. G., II, Eds.; The Electrochemical Society: Pennington, New Jersey, 1992; Vol. 92-1.

(4) Dewald, H. D. *Electroanalysis* **1991**, *3*, 145-155.

(5) *Passivity of Metals and Semiconductors*; Froment, M., Ed.; Elsevier: Amsterdam, 1983.

(6) Sharpe, L. R.; Heineman, W. R.; Elder, R. C. *Chem. Rev.* **1990**, *90*, 705-722.

(7) Dewald, H. D.; Watkins, J. W., II; Elder, R. C.; Heineman, W. R. *Anal. Chem.* **1986**, *58*, 2968-2975.

(8) Smith, D. A.; Heeg, M. J.; Heineman, W. R.; Elder, R. C. *J. Am. Chem. Soc.* **1984**, *106*, 3053-3054.

(9) Smith, D. A.; Elder, R. C.; Heineman, W. R. *Anal. Chem.* **1985**, *57*, 2361-2365.

(10) Igo, D. H.; Elder, R. C.; Heineman, W. R.; Dewald, H. D. *Anal. Chem.* **1991**, *63*, 2535-2539.

(11) Igo, D. H.; Elder, R. C.; Heineman, W. R. *J. Electroanal. Chem.* **1991**, *314*, 45-57.

(12) Villain, F.; Briois, V.; Castro, I.; Helary, C.; Verdaguer, M. *Anal. Chem.* **1993**, *65*, 2545-2548.

(13) Yoshitake, H.; Yamazaki, O.; Ota, K. *J. Electroanal. Chem.* **1994**, *371*, 287-290.

(14) Nagy, Z.; You, H.; Yonco, R. M.; Melendres, C. A.; Yun, W.; Maroni, V. A. *Electrochimica Acta* **1991**, *36*, 209-212.

(15) Herron, M. E.; Doyle, S. E.; Roberts, K. J.; Robinson, J.; Walsh, F. C. *Rev. Sci. Instrum.* **1992**, *63*, 950-955.

(16) Kordesch, M. E.; Hoffman, R. W. *Nucl. Instrum. Meth. Phys. Res.* **1984**, *222*, 347-350.

(17) Elder, R. C.; Lunte, C. E.; Rahman, A. F. M. M.; Kirchhoff, J. R.; Dewald, H. D.; Heineman, W. R. *J. Electroanal. Chem.* **1988**, *240*, 361-364.

(18) Capehart, T. W.; Corrigan, D. A.; Conell, R. S.; Pandya, K. I.; Hoffman, R. W. *Appl. Phys. Lett.* **1991**, *58*, 865-867.

(19) McBreen, J.; O'Grady, W. E.; Pandya, K. I.; Hoffman, R. W.; Sayers, D. E. *Langmuir* **1987**, *3*, 428-433.

(20) Tryk, D. A.; Bae, I. T.; Hu, Y.; Kim, S.; Antonio, M. R.; Scherson, D. A. *J. Electrochem. Soc.* **1995**, *142*, 824-828.

(21) Tryk, D. A.; Kim, S.; Hu, Y.; Xing, W.; Scherson, D. A.; Antonio, M. R.; Leger, V. Z.; Blomgren, G. E. *J. Phys. Chem.* **1995**, *99*, 3732-3735.

(22) Kim, S.; Bae, I. T.; Sandifer, M.; Ross, P. N.; Carr, R.; Woicik, J.; Antonio, M. R.; Scherson, D. A. *J. Am. Chem. Soc.* **1991**, *113*, 9063-9066.

(23) Pourbaix, M. *Atlas of Electrochemical Equilibria in Aqueous Solutions;* 2nd ed.; Cebelcor: Brussels, 1974, pp 183-197.

(24) Anderson, L. B.; Macero, D. J. *J. Phys. Chem.* **1963**, *67*, 1942.

(25) Biedermann, G.; Terjosin, G. S. *Acta Chem. Scand.* **1969**, *23*, 1896-1902.

(26) Biedermann, G.; Silber, H. B. *Acta Chem. Scand.* **1973**, *27*, 3761-3768.

(27) Bard, A. J.; Parsons, R.; Jordan, J. *Standard Potentials in Aqueous Solution*; Marcel Dekker: New York, 1985, pp 834.

(28) *SPEX Handbook of Sample Preparation and Handling*; 4 ed.; Obenauf, R. H.; Bostwick, R.; McCann, M.; McCormack, J. D.; Merriman, R.; Selem, S., Eds.; SPEX Sample Preparation: Metuchen, NJ, 1994, Ch 4.

(29) Antonio, M. R. In *XAFS Workshop: SRI'94*; Stony Brook, New York, 1994.

(30) Matsushita, T.; Hashizume, H. In *Handbook on Synchrotron Radiation*; E. E. Koch, Ed.; North-Holland: Amsterdam, 1983; Vol. 1A; pp 261-314.

(31) Lytle, F. W. In *Applications of Synchrotron Radiation*; H. Winick, D. Xian, M. H. Ye and T. Huang, Eds.; Gordon and Breach: New York, 1989; Vol. 4; pp 135-223.

(32) Krause, M. O.; Oliver, J. H. *J. Phys. Chem. Ref. Data* **1979**, *8*, 329-338.

(33) Lytle, F. W.; Greegor, R. B.; Marques, E. C. In *Proc. 9th Int. Congr. Catal. Calgary*; M. J. Phillips and M. Ternan, Eds.; The Chemical Institue of Canada: Ottawa, 1988; Vol. 5; pp 54-85.

(34) Lytle, F. W. *Ber. Bunsenges. Phys. Chem* **1987**, *91*, 1251-1257.

(35) Antonio, M. R.; Xue, J. S.; Soderholm, L. *J. Alloys Compounds* **1994**, *207/208*, 444-448.

(36) Antonio, M. R.; Soderholm, L. *Inorg. Chem.* **1994**, *33*, 5988-5993.

(37) Staub, U.; Antonio, M. R.; Soderholm, L.; Guillaume, M.; Henggeler, W.; Furrer, A. *Phys. Rev. B: Condens. Matter* **1994**, *50*, 7085-7091.

(38) Berry, F. J.; Marco, J. F.; Steel, A. T. *Hyperfine Interactions* **1994**, *83*, 347-350.

(39) Bazuev, G. V.; Finkel'shtein, L. D.; Samsonov, N. D.; Shveikin, G. P. *Russian J. Inorg. Chem.* **1987**, *32*, 158-159.

(40) Ravot, D.; Godart, C.; Achard, J. C.; Lagarde, P. In *Valence Fluctuations in Solids*; L. M. Falicov, W. Hanke and M. B. Maple, Eds.; North-Holland: Amsterdam, 1981; pp 423-426.

(41) Michels, G.; Junk, S.; Schlabitz, W.; Holland-Moritz, E.; Abd-Elmeguid, M. M.; Dünner, J.; Mewis, A. *J. Phys.: Condens. Matter* **1994**, *6*, 1769-1778.

(42) Wortmann, G. *Hyperfine Interactions* **1989**, *47*, 179-202.

(43) Wortmann, G.; Nowik, I.; Perscheid, B.; Kaindl, G.; Felner, I. *Phys. Rev. B: Condens. Matter* **1991**, *43*, 5261-5268.

(44) Bard, A. J.; Faulkner, L. R. *Electrochemical Methods. Fundamentals and Applications*; John Wiley & Sons: New York, 1980, Ch. 10.

(45) Antonio, M. R.; Soderholm, L., in preparation.

(46) Jensen, M.; Skanthakumar, S.; Soderholm, L.; Antonio, M. R., unpublished results.

(47) Meitzner, G.; Via, G. H.; Lytle, F. W.; Sinfelt, J. H. *J. Phys. Chem.* **1992**, *96*, 4960-4964.

(48) Röhler, J. In *Handbook on the Physics and Chemistry of Rare Earths*; K. A. Gschneidner Jr., L. Eyring and S. Hüfner, Eds.; North-Holland: Amsterdam, 1987; Vol. 10; pp 453-545.

(49) Lelieur, J. P.; Goulon, J.; Cortes, R.; Friant, P. *J. Phys. Chem.* **1984**, *88*, 3730-3734.

(50) Singhal, R. K.; Garg, K. B. *J. Magn. Magn. Mater.* **1992**, *116*, 238-248.

(51) Lissner, F.; Krämer, K.; Schleid, T.; Meyer, G.; Hu, Z.; Kaindl, G. *Z. anorg. allg. Chem.* **1994**, *620*, 444-450.

(52) Baba, T.; Hikita, S.; Koide, R.; Ono, Y.; Hanada, T.; Tanaka, T.; Yoshida, S. *J. Chem. Soc., Faraday Trans.* **1993**, *89*, 3177-3180.

(53) Cho, E. J.; Oh, S. J.; Imada, S.; Suga, S.; Suzuki, T.; Kasuya, T. *Phys. Rev. B: Condens. Matter* **1995**, *51*, 10146-10149.

(54) Han, M.; Oh, S. J.; Park, J. H.; Park, H. L. *J. Appl. Phys.* **1993**, *73*, 4546-4549.

(55) Schneider, W. D.; Laubschat, C.; Nowik, I.; Kaindl, G. *Phys. Rev. B* **1981**, *24*, 5422-5425.

(56) Mattheiss, L. F.; Dietz, R. E. *Phys. Rev. B* **1980**, *22*, 1663-1676.

(57) Fano, U.; Cooper, J. W. *Reviews of Modern Physics* **1968**, *40*, 441-507.

(58) Dieke, G. H. *Spectra and Energy Levels of Rare Earth Ions in Crystals*; Interscience Publishers: New York, 1968, pp 401.

(59) Hufner, S. *Optical Spectra of Transparent Rare Earth Compounds*; Academic Press: New York, 1978, pp 237.

(60) Wortmann, G.; Krone, W.; Sampathkumaran, E. V.; Kaindl, G. *Hyperfine Interactions* **1986**, *28*, 581-584.

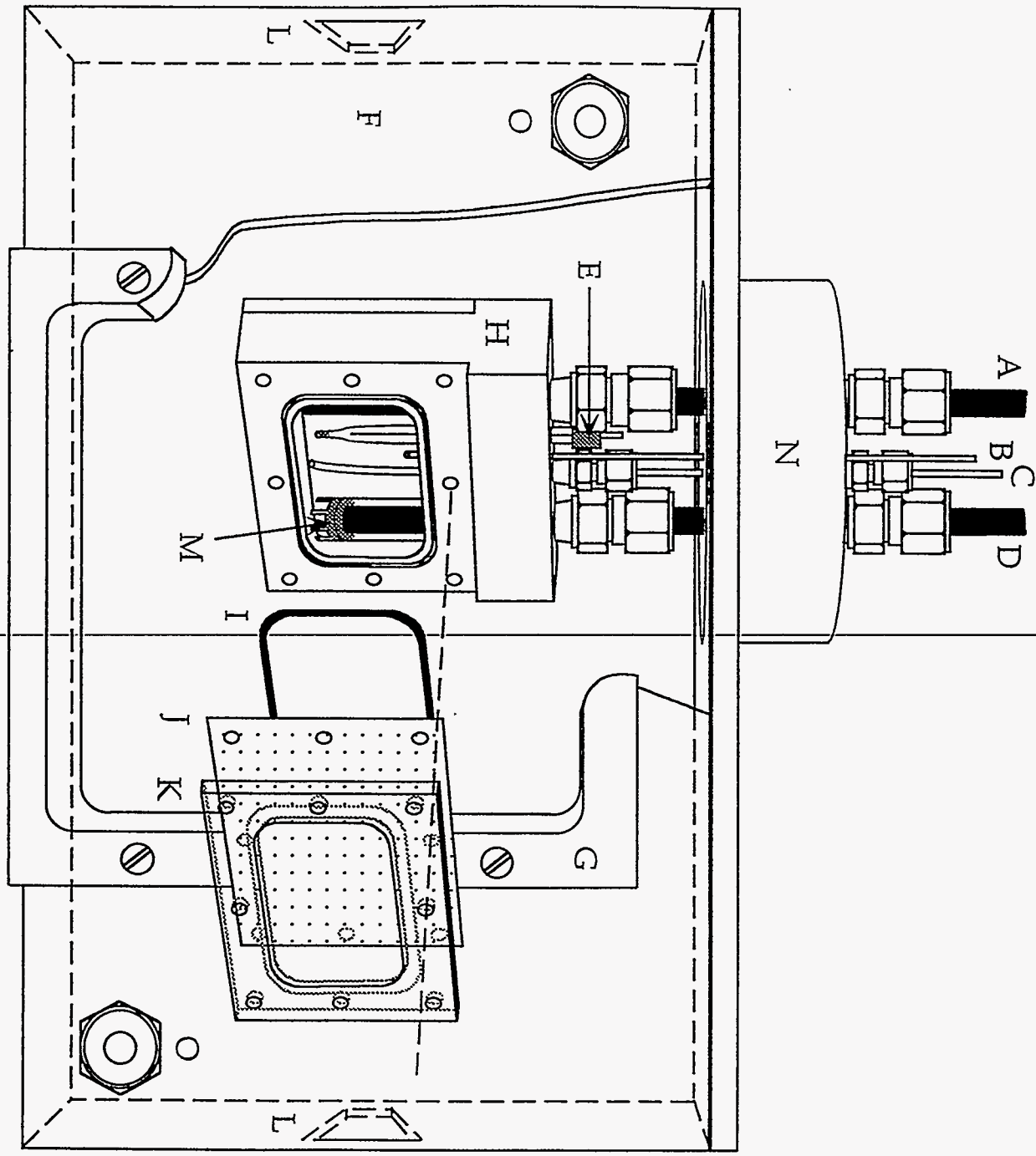

Antonio, Soderholm, Song
Figure 1

Antonio, Soderholm, Song
Figure 2

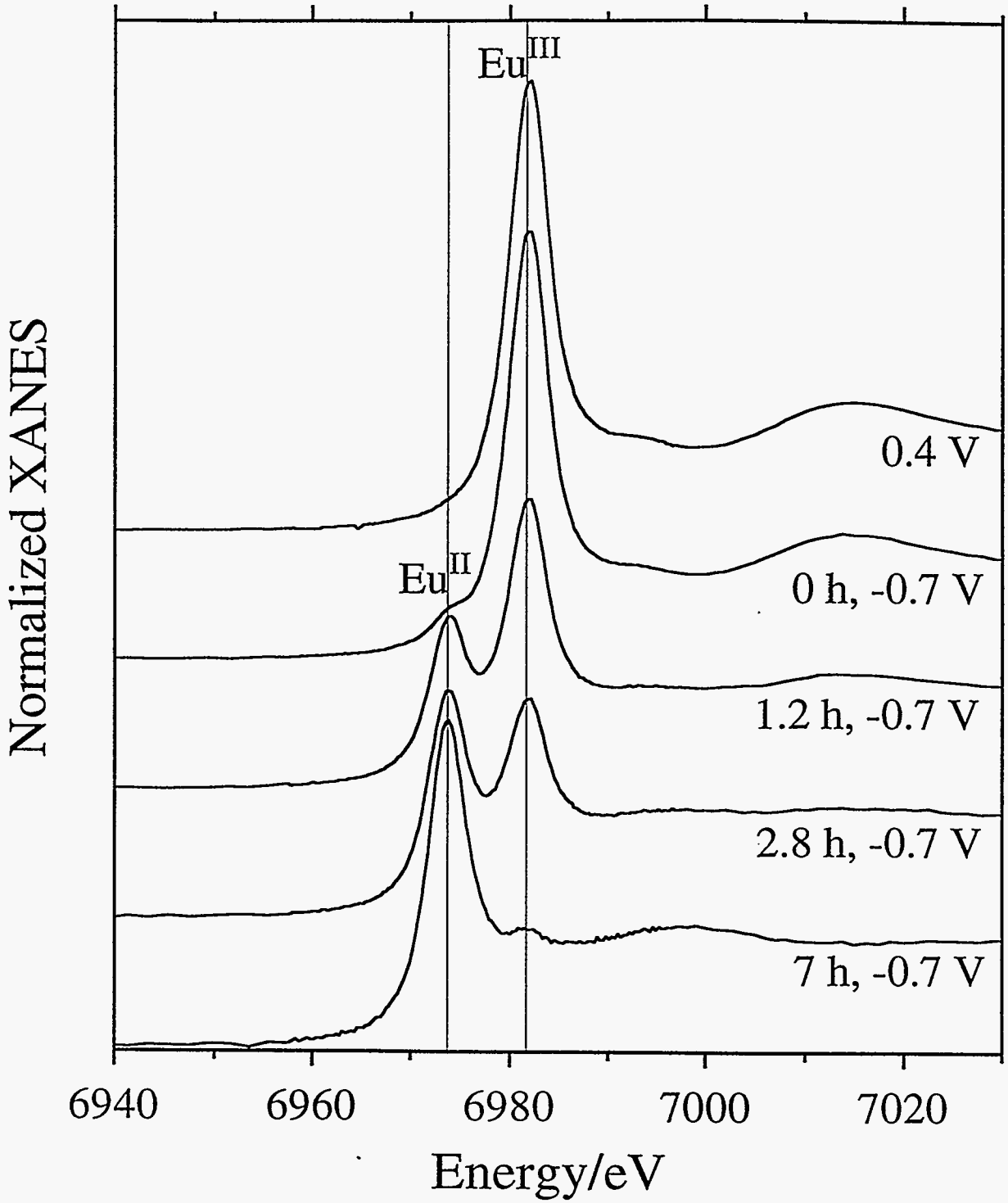

Figure 3
Antonio, Soderholm, Song